Hindawi
International Journal of Antennas and Propagation
Volume 2021, Article ID 4056424, 10 pages
https://doi.org/10.1155/2021/4056424

Research Article

A Low-Sidelobe-Level Variable Inclination Continuous Transverse Stub Antenna with a Nonlinear Slow-Wave Structure

Kexin Wang, Xue Lei, Jun Gao, Tianpeng Li, Siyu Tian, and Mingyang Zhao

Information Engineering, University Zhengzhou, Zhengzhou, China

Correspondence should be addressed to Kexin Wang; 201539252285@mail.scut.edu.cn

Received 17 August 2021; Revised 13 October 2021; Accepted 28 October 2021; Published 15 November 2021

Academic Editor: Paolo Burghignoli

Copyright © 2021 Kexin Wang et al. This is an open access article distributed under the Creative Commons Attribution License, which permits unrestricted use, distribution, and reproduction in any medium, provided the original work is properly cited.

The sidelobe level (SLL) is an essential performance factor for satellite communication antennas. A low-SLL design can effectively suppress adjacent satellite interference. A low-SLL design method for a variable inclination continuous transverse stub (VICTS) antenna is proposed in this paper. The VICTS antenna is composed of three rotatable parts: a feeding plate, a radiation plate, and a polarization plate. The radiation plate comprises two groups of stubs with different radiation ratios. Combined with the nonlinear slow-wave structure attached to the feeding plate, the radiation ratio of the unit can be adjusted. The aperture field of the VICTS antenna using this method can be tapered in order to suppress the SLL. To verify the effectiveness of this method, the antenna prototype is fabricated and measured in a microwave anechoic chamber. The simulation and the measurement are in good agreement. The reflection coefficient of the antenna is kept below −15 dB and between 13.75 GHz and 14.5 GHz. When the radiation plate and the feeding plate rotate relative to each other, the pattern beam can be scanned from 5° to 70°. In the scanning range, the typical SLL can reach −18 dB.

1. Introduction

Satellite communication [1–3] is a highly specialized technology field and one of the important methods of modern communication and informatization. Satellite communication has the advantages of wide coverage, large capacity, and high quality. With the widespread application of high-throughput satellites [4] and low-orbit satellites [5], satellite communication has ushered in a new round of advanced development. Mobile carriers such as airplanes, vehicles, and ships can be connected to satellite networks by installing satellite interconnect antenna terminals. This has caused mobile communication systems [6, 7] to play an increasingly important role in military communications and emergency communications. One of the key technologies of a satellite mobile communication system is antenna technology. Mobile communication antenna technology with high gain, a low sidelobe level (SLL) [8–10], and a low profile has become one of the research hotspots in satellite mobile communication technology.

Based on their structural forms, mobile communication antennas can be divided into reflector antennas [11, 12], lens antennas [13–15], and array antennas [16–18]. Reflector antennas have the best performance. It is easy to increase their apertures to achieve high gain. At the same time, a reflector antenna has a simple structure and few radio frequency (RF) devices, so it is easy to achieve the common use of a transceiver. However, the high profile is the biggest disadvantage, so a reflector antenna cannot be applied in a high-speed mobile carrier. The gain of a dielectric lens antenna does not result in a decrease in beam scanning, and it is easy to achieve multifrequency bands. However, the antenna structure is complex, and its efficiency is reduced at high frequency. A planar array antenna has a very low profile and high RF integration. The pitch angle can range from 0° to 90°. For a single-chip antenna, the aperture is not easy to enlarge, and the feed and RF components are more complex. For multicomponent antennas, the performance is degraded at high and low elevation angles, and the cost is not negligible.

tA continuous transverse stub (CTS) [19–21] antenna is developed from a waveguide slot array antenna, which simplifies the difficulty with feeding and processing and has more development space. The CTS antenna has stubs on the upper surface of the parallel plate waveguide. The stub has the characteristics of a wide band, high radiation ratio, low loss, and compact structure. A variable inclination continuous transverse stub (VICTS) antenna is based on a CTS antenna. The radiation and feeding structures of the VICTS antenna can rotate relative to each other. Because of its low profile and simple structure, a series-fed VICTS antenna is very suitable for communication in motion. However, it is difficult to control the aperture distribution of a series-fed VICTS antenna. In [22], the authors changed the radiation ratio of a stub by changing its width, and the radiation ratio can be maintained at 10%–28%. The space between the radiation plate and the feeding plate is filled with the dielectric, which increases the loss of the antenna. This method cannot control the aperture field distribution of the antenna well. Therefore, the SLL of the antenna reaches −9 dB. In [23], the authors adjusted the radiation ratio of the stub by adding matching grooves. By adjusting the depth and position of the groove to adjust the radiation ratio, the radiation ratio can be maintained between 7.69% and 100%. However, the SLL is still −14 dB. Due to different parameters of stubs, the processing difficulty of engineering manufacturing is greatly increased. Phase-shifted surface technology is used to steer an antenna beam [24]. A low sidelobe is obtained by using a horn as the feed. However, the overall height of the antenna is increased due to the horn feed. By using the patch as the feed [25], the height of the antenna can be effectively reduced. The beam is steered via the rotation of the two sawtooth time-delay (STD) metasurfaces. The feed of the VICTS antenna is a line source. The relative rotation of the radiation plate with the feed produces a phase difference to steer the beam. The prototype and the basic principles of the VICTS antenna are described in some ThinKom patents, but there is no low-SLL design method for the VICTS antenna in the publicly available literature.

Some attempts have been made to reduce the sidelobe level of a VICTS antenna in my previous work [26]. The aperture field distribution of an antenna cannot be well controlled by changing only the number of stubs. The SLL is slightly suppressed, and the prototype is not processed for measurement. In this research, a low-SLL VICTS antenna operating at 13.75–14.5 GHz is designed. Because of its unique beam characteristics, the antenna has almost no sidelobe on the orbit arc of the target satellite. The radiation ratio of the stub is changed by adjusting the height of the parallel plate waveguide and the width of the slot. The SLL is suppressed by a double nonlinear structure. One feature of the structure is that the height of the parallel plate waveguide changes nonlinearly. Another feature is that the height of the slow-wave structure has a nonlinear relationship with the height of the parallel plate waveguide. The VICTS antenna is introduced in the second section of this paper. The third section describes the design process of a stub and a slow-wave structure. The fourth section describes the simulation and measurement results. The fifth section describes the conclusions.

2. Introduction of the VICTS Antenna Model

The model of the VICTS antenna is shown in Figure 1(a). The main structure of the antenna is divided into two parts: the feeding plate and the radiation plate. The two plates maintain a small gap to facilitate relative rotation through the servo control system. The two-dimensional beam scanning of the antenna can be achieved with the rotation of two plates. The relative rotation of the two plates can steer the elevation of the pattern beam. The azimuth scanning can be achieved by rotating the two plates at the same time [27]. The polarization plate is composed of multiple metal grids that are placed directly above the radiation plate (not shown in the figure). The function of the polarization plate is to adjust the polarization of the antenna so that the main polarization of the antenna matches the main polarization of the satellite. Since the research focus of this paper is the low-SLL design and the polarization plate has no effect on the antenna pattern, the polarization plate is not described in detail.

The beam scanning principle of the VICTS antenna is to change the phase distribution of the slot. When the two plates rotate relative to each other, the equal phase plane of the electromagnetic wave between the parallel plates forms a certain angle with the slot. Therefore, the antenna requires a linear source. The main view of the feeding plate is shown in Figure 1(b). One side of the feeding plate is a 1–12 power divider, and the phase of each output port is kept the same to generate a linear source. On the other side, the red dotted line area is a nonlinear slow-wave structure attached to the bottom of the parallel plate. The slow-wave structure is made of lightweight plastic processed with electroplating, with an equivalent dielectric constant of 1.14 and no loss. It can be seen from Figure 1(c) that the height of the parallel plate waveguide changes nonlinearly, and this height change can flexibly control the radiation ratio of the unit. The slow-wave structure can change the propagation constant between parallel plates to suppress the generation of the grating lobes. Compared with the filled medium, the slow-wave structure can reduce the loss of the antenna.

The radiation plate consists of two groups of stubs with a matching step. The period of the two groups of stubs stays the same, but the radiation ratio is different. The reasons for not using three or more groups of stubs are as follows. First, through the combination of two stubs, the radiation ratio range of the unit is large enough to suppress the SLL. Second, multiple groups of stubs will increase the difficulty of antenna design and processing, which is not conducive to reducing the cost of the antenna.

3. Antenna Design

3.1. Design of the Stub. As the main radiator of the antenna, the design of the stub is very important. As a passive phased-array antenna, the VICTS antenna does not have a large number of T/R components. Therefore, the radiation ratio of stubs should be easily adjusted. The details of the stub are shown in Figure 2. In order to suppress the generation of the grating lobe, the period d of the stub should be less than the

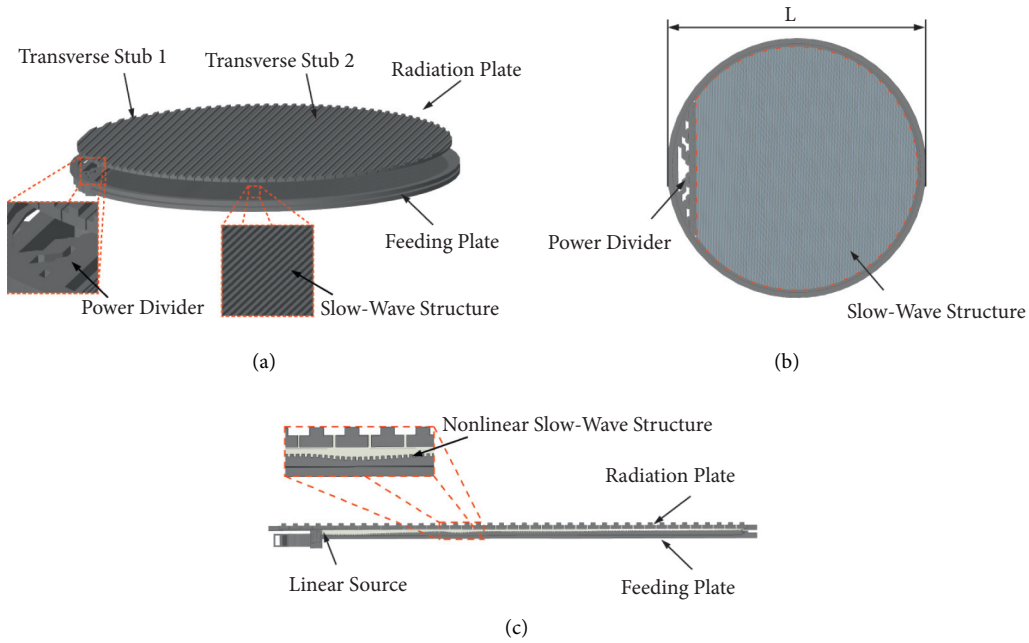

Figure 1: Overview of the VICTS antenna. (a) 3D view. (b) Top view of the feeding plate. (c) Sectional view.

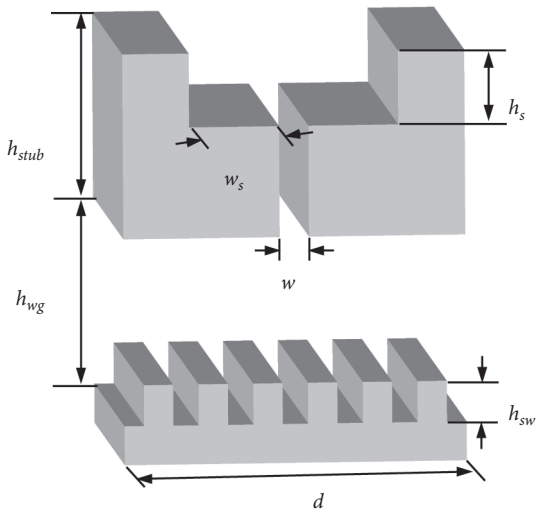

Figure 2: 3D diagram of the stub.

minimum operating wavelength. The active impedance of the stub array is matched by a step with a height of h_s. In [28], the influences of each parameter of the stub on the stub's radiation ratio are given. The radiation ratio of the stubs is directly proportional to w and inversely proportional to h_{wg}. The maximum operating frequency of the antenna is $f_{\max} = 14.5$ GHz, the equivalent dielectric constant of the slow-wave structure is $\epsilon_e = 1.14$, and the half wavelength $\lambda_{\min}$ is calculated to be 9.65 mm. Therefore, the maximum value of h_{wg} is 9.6 mm. According to engineering experience, in order to prevent the radiation plate and the feeding plate from coming into contact with each other when rotating, the minimum value of h_{wg} is 3.6 mm. In order to increase the range of the radiation ratio, two groups of radiation stubs with different parameters w are selected. Their parameters are listed in Table 1. The maximum and minimum radiation ratios of a single stub are shown in Figure 3(a). The maximum radiation ratio of stub 1 is 2% higher than that of stub 2. The purpose of this design is that it is convenient for the subsequent design of the radiation ratio of the stubs which can be continuously adjusted. At the same time, the variation trend of h_{wg} with adjacent stubs can be gentler.

3.2. Height of the Parallel Plate Waveguide. As the key parameter to control the radiation ratio of the stub, the change of h_{wg} is the main design factor for suppressing the SLL. There are two nonlinear relationships. One relationship is that the height of slow-wave structure h_{sw} is nonlinear with h_{wg}, which keeps the propagation constant between the parallel plates unchanged [29]. The other relationship is that h_{wg} is nonlinear with the propagation distance. In order to eliminate the influence of the slow-wave structure on the radiation ratio of the stub, the nonlinear slow-wave structure is added to the unit while simulating the influence of h_{wg} on the radiation ratio. The relationship between the radiation ratio and h_{wg} of the two groups of stubs at 14 GHz is shown in Figure 3(b). The fitting toolbox of MATLAB is used to fit the two curves.

When the two plates do not rotate relative to each other, the phase on a single stub remains unchanged. In this case, the radiation pattern of the VICTS antenna can be calculated with one-dimensional linear array theory. The feed structure of the antenna is a 1–12 equal ratio power divider, so the ideal line source is used as the feed source in the calculation model. In order to simplify the calculation, the reflection caused by the outer ring of the antenna is not considered, so the boundary is set as the magnetic boundary. The total number of slots N is 33, in which the number of slot 1 is N_1

Table 1: Parameters of the two stubs (unit: mm).

	h_{stub}	d	w_s	w	h_s
Stub 1	9.2	18	5	0.9	3.8
Stub 2	9.2	18	4.5	1.5	3.8

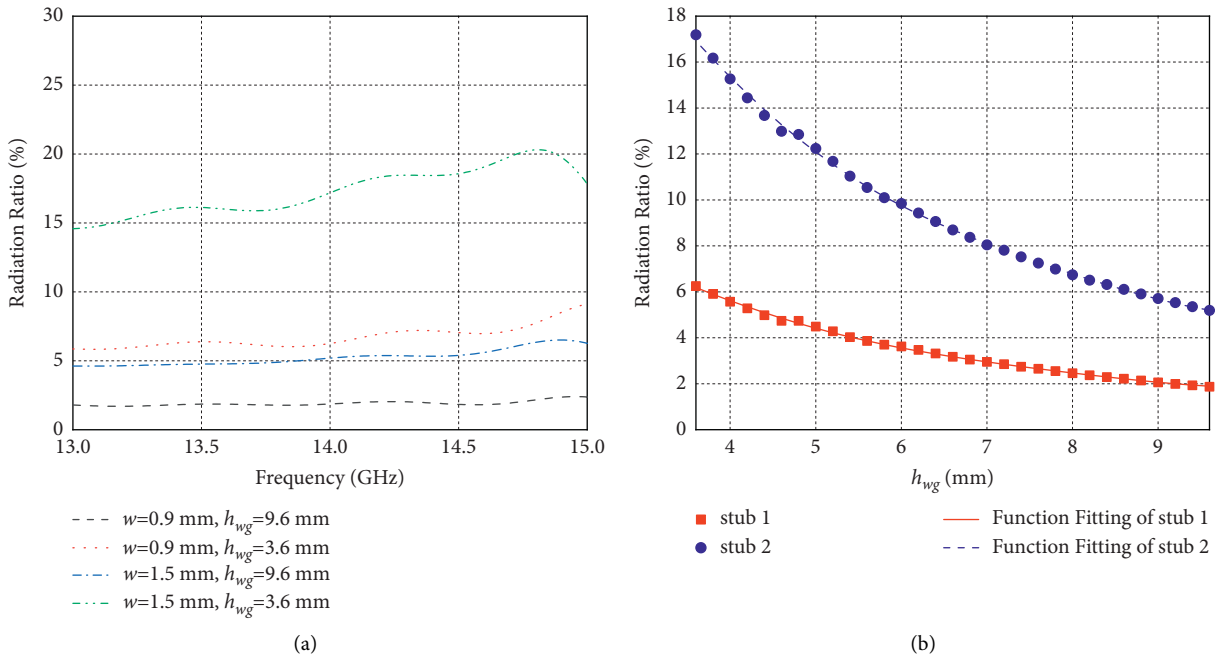

Figure 3: Radiation ratio of stubs. (a) Radiation ratio at different frequencies. (b) Relationship between radiation ratio and h_{wg} at 14 GHz.

and the number of slot 2 is N_2. In order to make the peak of the antenna aperture field appear in the center, the radiation ratio of the stub in the center should be increased. Hence, here, N_1: N_2 = 1: 2 is taken. The height of the parallel plate waveguide corresponding to each slot is recorded as h_i. The excitation amplitude at each slot can be expressed as [30]

$$\dot{I}_n = \sqrt{\prod_{i=1}^{n}(1-\eta_{i-1})\eta_i e^{jk\sqrt{\epsilon_e}dn}}, \quad n = 1, \ldots, N_1 + N_2, \quad (1)$$

where $k = 2\pi f/c$, f is the operating frequency, c is the speed of light in a vacuum, and ϵ_e is the equivalent dielectric constant of the slow-wave structure. The radiation ratio η_i can be expressed as

$$\eta_i = u(N_1 - i) f_1(h) + u(i - N_1) f_2(h). \quad (2)$$

Here, $u(\bullet)$ is the step function. $f_1(\bullet)$ and $f_2(\bullet)$ are the fitting functions described above. Therefore, the antenna radiation pattern can be calculated with the following formula [31]:

$$F(\theta) = \sum_{n=1}^{N_1+N_2} C\dot{I}_n e^{jkdn\sin\theta}. \quad (3)$$

As a global optimization algorithm, a genetic algorithm [32–34] does not easily fall into the trap of a local minimum. Therefore, a genetic algorithm is used as an optimization tool to optimize the SLL of the antenna pattern. The solution process is shown in Figure 4. The height of the nonlinear slow-wave structure should change slowly in order to avoid a large amount of energy not radiating, which helps to reduce the reflection coefficient.

The optimization results of h_i and the aperture field distribution of the overall antenna model calculated with MATLAB are shown in Figure 5. The continuous height of the parallel plate waveguide can be obtained with a smooth interpolation algorithm. The electric field distribution perpendicular to the direction of the stub is shown by the red solid line in Figure 5. Because the minimum radiation ratio of the stub is designed to be small enough, the electric field amplitude at both ends of the antenna aperture can be suppressed below 10 dB. With the reasonable number of stubs and the curve of the height of the planar waveguide, the aperture field of the antenna can be tapered to suppress the SLL. The electric field amplitude of the antenna aperture center can reach more than 30 dB. The theoretical pattern calculated with formula (3) is shown in Figure 6, and the SLL can reach −21.8 dB.

4. Result

The VICTS antenna is modeled and simulated in CST software, and satisfactory performance is achieved in the range of 13.75–14.5 GHz. In order to verify the performance of the antenna, the prototype is fabricated and measured in

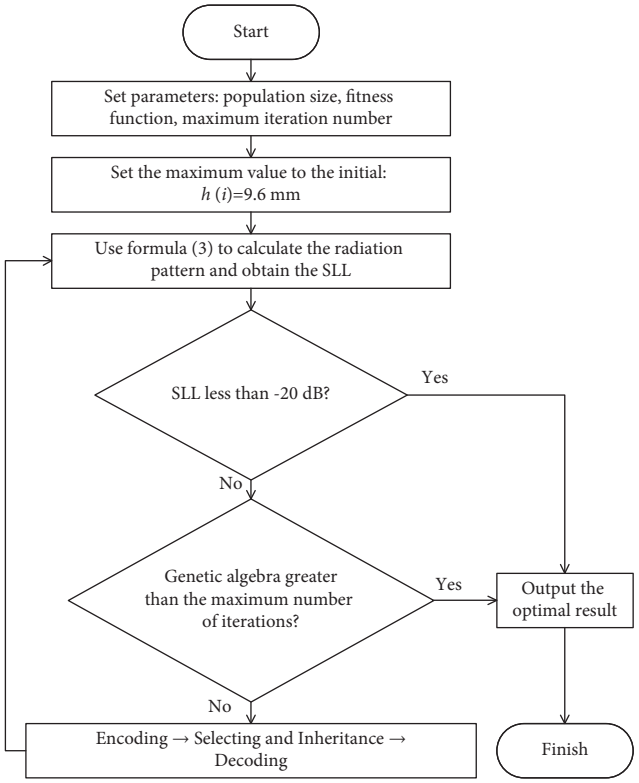

Figure 4: Flowchart of the genetic algorithm.

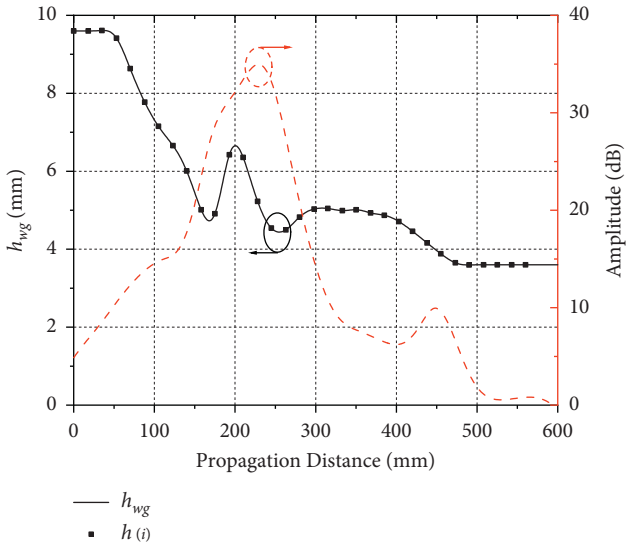

Figure 5: Height variation of the parallel plate waveguide (solid line) and antenna aperture field distribution (dotted line).

the microwave anechoic chamber. The near-field measurement system is shown in Figure 7. The main structure of the antenna is made of lightweight materials that are electroplated. The total height of the radiation plate and the feeding plate of the antenna is 25 mm (1.25λ). These two parts are affixed to the central principal axis, so they can be rotated continuously to achieve the continuous scanning of the antenna beam. When the relative rotation angle γ stays at 0°,

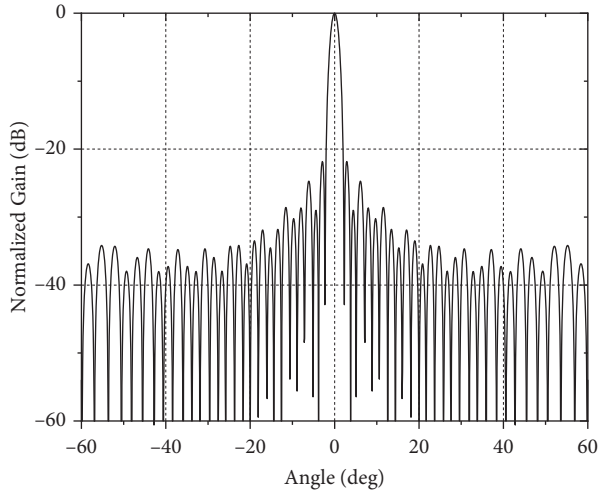

Figure 6: The calculated radiation pattern based on the optimization results.

Figure 7: Antenna prototype and measurement system.

10°, 20°, 30°, and 40°, the performance is measured. Due to the symmetry of the antenna structure, the radiation pattern is symmetrical when the rotation angle is the opposite.

The reflection coefficient of the antenna input port is shown in Figure 8. The simulated and measured reflection coefficients of the antenna for different γ are shown by the solid line and the dotted line, respectively. The reflection coefficient of the antenna is suppressed below −15 dB in the band of 13–15 GHz. The difference between the simulation and the measurement is due to the inevitable machining tolerance. The radiation efficiency of the antenna can reach 95%.

The 3D far-field simulation pattern of the antenna at 14 GHz and $\gamma = 0°$ is shown in Figure 9(a). The pattern of the

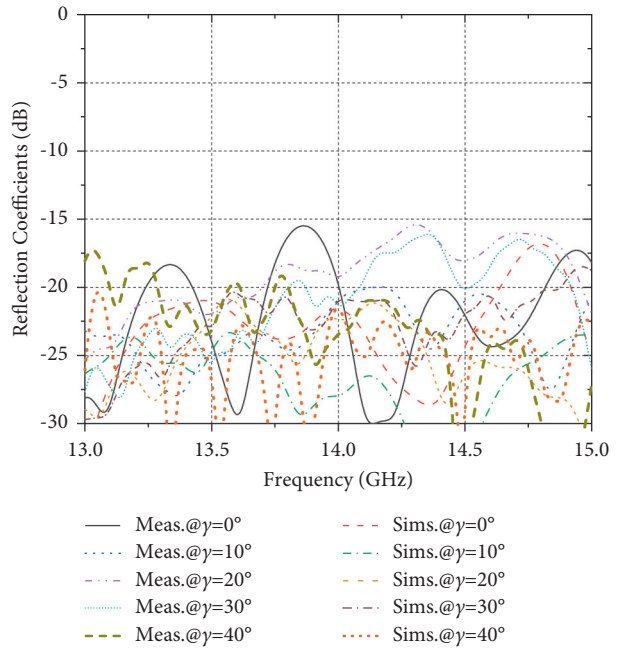

Figure 8: Simulation and measurement of the reflection coefficient of the input port.

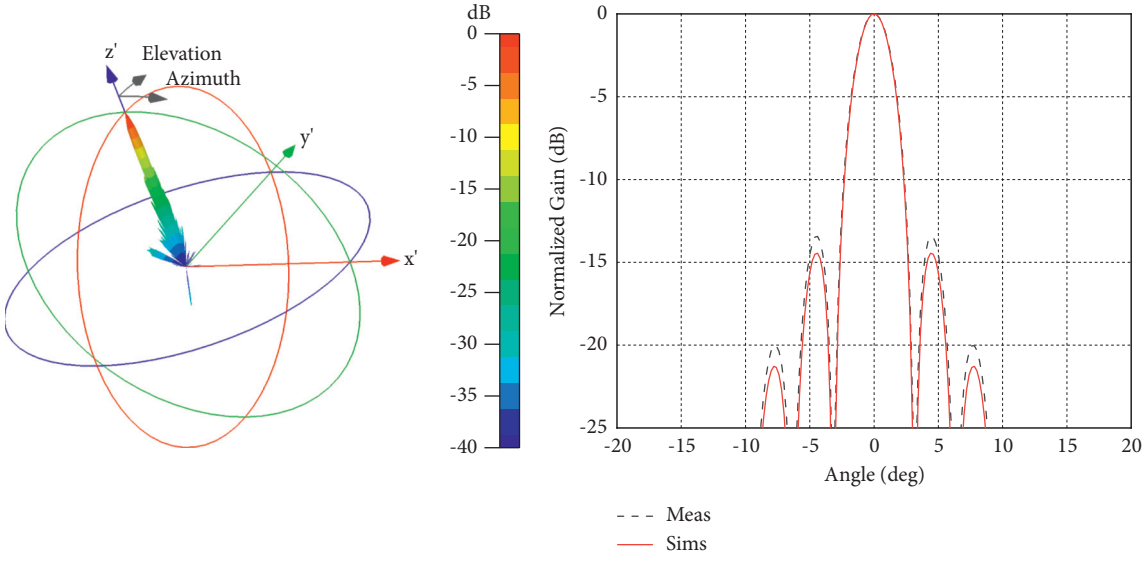

(a) (b)

Figure 9: Continued.

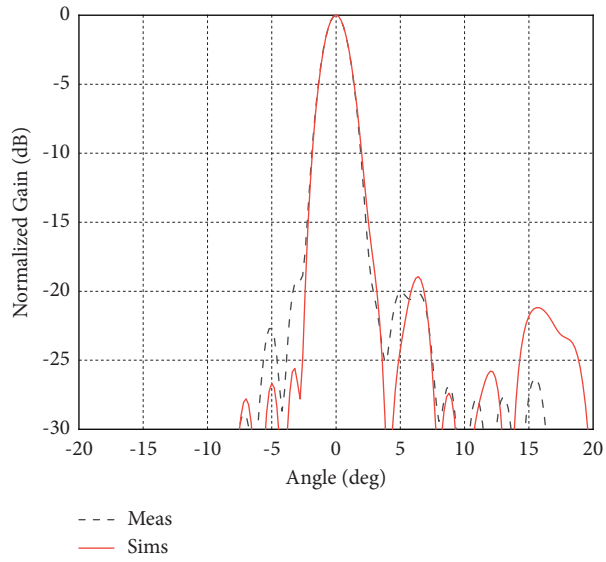

(c)

Figure 9: Radiation pattern at 14 GHz and $\gamma = 0^{\circ}$. (a) Far-field pattern. (b) Elevation plane. (c) Azimuth plane.

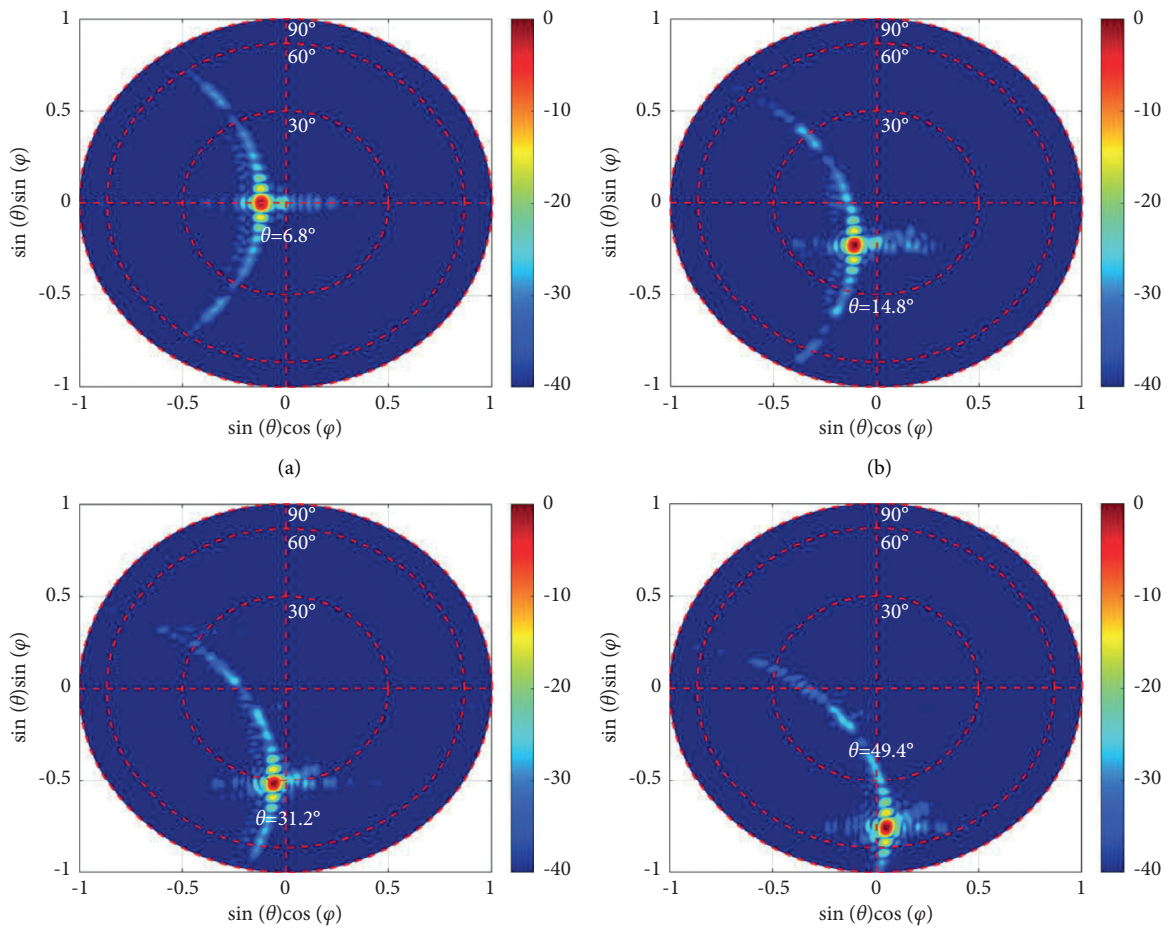

(a) (b) (c) (d)

Figure 10: Continued.

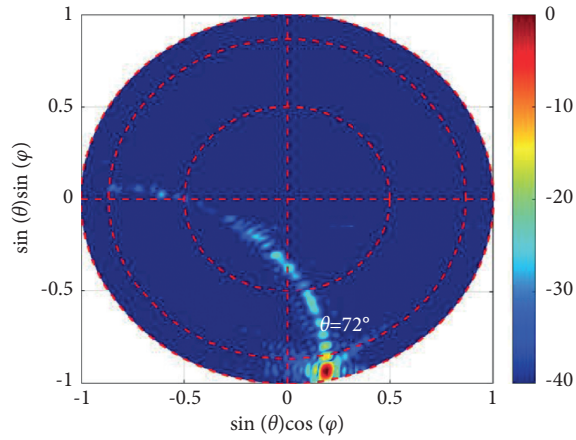

(e)

Figure 10: Simulation pattern of the VICTS antennas at 14 GHz. (a) $\gamma = 0^{\circ}$. (b) $\gamma = 10^{\circ}$. (c) $\gamma = 20^{\circ}$. (d) $\gamma = 30^{\circ}$. (e) $\gamma = 40^{\circ}$.

VICTS antenna is not omnidirectional in the azimuth plane, but is rather a typical crossbeam, which is consistent with the calculation result of the closed expression of the VICTS pattern [27]. The corresponding cutting patterns of the elevation and azimuth planes are shown in Figures 9(b) and 9(c). The azimuth plane and the elevation plane correspond to the $\phi = 0^{\circ}$ and $\phi = 90^{\circ}$ cuts, respectively. The main lobe of the simulation and the measurement cutting pattern of the elevation plane coincide completely, and there is a slight difference in the sidelobe. The elevation plane pattern depends on the power division feed network. The antenna is fed by equal power division without a low-SLL design, so the simulation SLL reaches −14.5 dB, and the measurement result reaches −13.4 dB. The radiation pattern of the azimuth plane is controlled by the combination design of the nonlinear slow-wave structure and the stubs. The SLL of the simulated azimuth plane is −18.9 dB, and the measured value reaches −19.2 dB. The electrical size of the slow-wave structure is too large (25λ at 14 GHz), so the very small machining tolerance will gradually accumulate, which has an important impact on the far-field pattern. However, the low SLL of the measured pattern still shows that the design has achieved obvious results.

The simulated scanning performance of the antenna at 14 GHz is shown in Figure 10. When the rotation angle γ changes from 0° to 40°, the scanning angle of the antenna can cover 5° to 70°. The period of the stubs is 18 mm, and the equivalent dielectric constant of the slow-wave structure is 1.14. Therefore, when $\gamma = 0$, the phase difference is 323°. At this time, according to the theory of a uniform linear array [31], it can be calculated that the beam direction at 14 GHz is 6.9°. Due to the frequency scanning characteristics of the antenna, the minimum pitch angle of the antenna can reach 5°. The SLL remains low throughout the scanning range, as shown in Figure 11. When the pattern is close to the normal radiation, the SLL can reach −19.2 dB. As the beam direction deviates from the normal direction, the SLL increases gradually. When the beam elevation angle reaches 70°, the SLL can still reach −17.4 dB. The period of the stubs is changed so that the phase difference between two adjacent

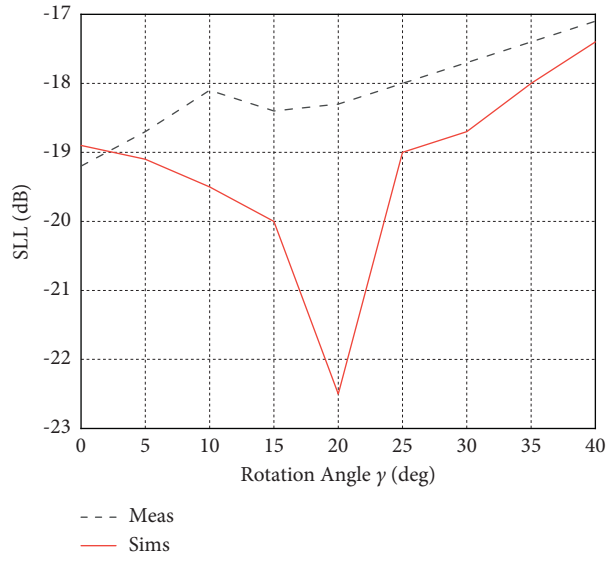

Figure 11: SLL at different rotation angles.

stubs can be 360°. In this case, when $\gamma = 0^{\circ}$, the antenna has normal radiation. With the increase of γ, the elevation angle of the beam point can even reach 90°, but at this time, the gain of the antenna will decrease, and the SLL will be seriously deteriorated so that it cannot be used for satellite communication.

5. Conclusions

A VICTS antenna with a low-SLL design is presented in this paper. The antenna prototype works in the range of 13.75–14.5 GHz. The antenna comprises a radiation plate and a feeding plate that can rotate relative to each other. The relative and common rotations of the two parts can achieve the scanning of elevation and azimuth, respectively. The radiation plate is composed of two groups of stubs with different radiation ratios. A double nonlinear slow-wave structure is attached to the feeding plate. The aperture field

distribution of the antenna can be controlled as a taper distribution using this method. The electric amplitude in the center of the antenna aperture can reach 30 dB, while it is only 5 dB at the side of the antenna. The results of the measurement and the simulation are in good agreement. The beam scanning range of the antenna can reach 5°–70°. The reflection coefficient of the antenna is less than −15 dB in the range of the working frequency and the scanning range. The SLL of the antenna can reach −19.2 dB at $\gamma = 0°$ and −17.4 dB at $\gamma = 40°$. The design method proposed in this paper can effectively reduce the SLL of the VICTS antenna. Only two groups of stubs are used to reduce the complexity and cost of antenna processing, which has great practical value.

Data Availability

The data used to support the findings of this study can be obtained by contacting the corresponding author via e-mail (201539252285@mail.scut.edu.cn).

Conflicts of Interest

The authors declare that they have no conflicts of interest.

References

[1] J. Su, S. Yang, H. Xu, and X. Zhou, "A stackelberg differential game based bandwidth allocation in satellite communication network," *China Communications*, vol. 15, no. 8, pp. 205–214, 2018.

[2] L. You, K.-X. Li, J. Wang, X. Gao, X.-G. Xia, and B. Ottersten, "Massive mimo transmission for leo satellite communications," *IEEE Journal on Selected Areas in Communications*, vol. 38, no. 8, pp. 1851–1865, 2020.

[3] S. Arnon and N. S. Kopeika, "Laser satellite communication network-vibration effect and possible solutions," *Proceedings of the IEEE*, vol. 85, no. 10, pp. 1646–1661, 1997.

[4] K. Kaneko, H. Nishiyama, N. Kato, A. Miura, and M. Toyoshima, "Construction of a flexibility analysis model for flexible high-throughput satellite communication systems with a digital channelizer," *IEEE Transactions on Vehicular Technology*, vol. 67, no. 3, pp. 2097–2107, 2018.

[5] R. Marchand, "PTetra, a tool to simulate low orbit satellite-plasma interaction," *IEEE Transactions on Plasma Science*, vol. 40, no. 2, pp. 217–229, 2012.

[6] L. Liuyan Han and N. Nan Hua, "A distributed time synchronization solution without satellite time reference for mobile communication," *IEEE Communications Letters*, vol. 17, no. 7, pp. 1447–1450, 2013.

[7] D. Raychaudhuri and N. B. Mandayam, "Frontiers of wireless and mobile communications," *Proceedings of the IEEE*, vol. 100, no. 4, pp. 824–840, 2012.

[8] Y.-W. Wu, Z. Jiang, and Z.-C. Hao, "A 400-ghz low cost planar leaky-wave antenna with low sidelobe level and low cross-polarization level," *IEEE Transactions on Terahertz Science and Technology*, vol. 10, no. 4, pp. 427–430, 2020.

[9] M. T. Mu and Y. J. Cheng, "Low-sidelobe-level short leaky-wave antenna based on single-layer pcb-based substrate-integrated image guide," *IEEE Antennas and Wireless Propagation Letters*, vol. 17, no. 8, pp. 1519–1523, 2018.

[10] J. Yin, Q. Wu, C. Yu, H. Wang, and W. Hong, "Low-sidelobe-level series-fed microstrip antenna array of unequal interelement spacing," *IEEE Antennas and Wireless Propagation Letters*, vol. 16, pp. 1695–1698, 2017.

[11] R. Chantalat, C. Menudier, M. Thevenot, T. Monediere, E. Arnaud, and P. Dumon, "Enhanced ebg resonator antenna as feed of a reflector antenna in the ka band," *IEEE Antennas and Wireless Propagation Letters*, vol. 7, pp. 349–353, 2008.

[12] J. G. Meana, J. A. Martinez-Lorenzo, M. A. Arias, F. Las-Heras, and A. G. Pino, "A shaped and reconfigurable reflector antenna with low sidelobe level for cellular wireless communications," *IEEE Antennas and Wireless Propagation Letters*, vol. 6, pp. 627–630, 2007.

[13] K. Zhang, Y. Yuan, D. Zhang et al., "Phase-engineered metalenses to generate converging and non-diffractive vortex beam carrying orbital angular momentum in microwave region," *Optics Express*, vol. 26, no. 2, pp. 1351–1360, 2018.

[14] Y. Chen, L. Chen, J.-F. Yu, and X.-W. Shi, "A c-band flat lens antenna with double-ring slot elements," *IEEE Antennas and Wireless Propagation Letters*, vol. 12, pp. 341–344, 2013.

[15] M. K. T. Al-Nuaimi, W. Hong, and Y. Zhang, "Design of high-directivity compact-size conical horn lens antenna," *IEEE Antennas and Wireless Propagation Letters*, vol. 13, pp. 467–470, 2014.

[16] S. J. Li, Y. B. Li, L. Zhang et al., "Programmable controls to scattering properties of radiation array," *Laser & Photonics Reviews*, vol. 15, no. 2, Article ID 2000449, 2021.

[17] R. Lian, Z. Wang, Y. Yin, J. Wu, and X. Song, "Design of a low-profile dual-polarized stepped slot antenna array for base station," *IEEE Antennas and Wireless Propagation Letters*, vol. 15, pp. 362–365, 2016.

[18] Z. Wang, G.-x. Zhang, Y. Yin, and J. Wu, "Design of a dual-band high-gain antenna array for wlan and wimax base station," *IEEE Antennas and Wireless Propagation Letters*, vol. 13, pp. 1721–1724, 2014.

[19] S. Zhou, M. Ettorre, and A. Grbic, "An 8×4 continuous transverse stub array fed by coaxial ports," *IEEE Antennas and Wireless Propagation Letters*, vol. 18, no. 6, pp. 1303–1307, 2019.

[20] X. Lu, S. Gu, X. Wang, H. Liu, and W. Lu, "Beam-scanning continuous transverse stub antenna fed by a ridged waveguide slot array," *IEEE Antennas and Wireless Propagation Letters*, vol. 16, pp. 1675–1678, 2017.

[21] Y. Lu, Q. You, Y. Wang, Y. You, J. Huang, and K. Wu, "Millimeter-wave low-profile continuous transverse stub arrays with novel linear source generators," *IEEE Transactions on Antennas and Propagation*, vol. 67, no. 2, pp. 988–997, 2019.

[22] R. S. Hao, Y. J. Cheng, and Y. F. Wu, "Shared-aperture variable inclination continuous transverse stub antenna working at k- and ka-bands for mobile satellite communication," *IEEE Transactions on Antennas and Propagation*, vol. 68, no. 9, pp. 6656–6666, 2020.

[23] K. Tekkouk, J. Hirokawa, R. Sauleau, and M. Ando, "Wide-band and large coverage continuous beam steering antenna in the 60-ghz band," *IEEE Transactions on Antennas and Propagation*, vol. 65, no. 9, pp. 4418–4426, 2017.

[24] N. Gagnon and A. Petosa, "Using rotatable planar phase shifting surfaces to steer a high-gain beam," *IEEE Transactions on Antennas and Propagation*, vol. 61, no. 6, pp. 3086–3092, 2013.

[25] M. U. Afzal and K. P. Esselle, "Steering the beam of medium-to-high gain antennas using near-field phase transformation," *IEEE Transactions on Antennas and Propagation*, vol. 65, no. 4, pp. 1680–1690, 2017.

[26] K. Wang, X. Lei, J. Gao, T. Li, and M. Zhao, "A low-sidelobe-level variable inclination continuous transverse stub antenna with two-types stubs," in *Proceedings of the 2021 IEEE 4th Advanced Information Management, Communicates, Electronic and Automation Control Conference*, vol. 4, pp. 1554–1558, Chongqing, China, June 2021.

[27] B. G. Porter, "Closed form expression for antenna patterns of the variable inclination continuous transverse stub," in *Proceedings of the 2010 IEEE International Symposium on Phased Array Systems and Technology*, p. 164, Waltham, MA, USA, November 2010.

[28] H. Qiu, X.-X. Yang, Y. Yu, T. Lou, Z. Yin, and S. Gao, "Compact beam-scanning flat array based on substrate-integrated waveguide," *IEEE Transactions on Antennas and Propagation*, vol. 68, no. 2, pp. 882–890, 2020.

[29] J. Gao, X. Lei, G.-H. Chen, Y. Zhang, and J.-M. Wu, "Design of the variable inclination continuous transverse stub antenna based on rectangular grating slow-wave structure," *International Journal of Antennas and Propagation*, vol. 2018, Article ID 5793535, 7 pages, 2018.

[30] K. Wang, X. Lei, J. Gao, T. Li, and M. Zhao, "A mathematical model for sidelobe level optimization of variable inclination continuous transverse stub antenna," *International Journal of Microwave and Wireless Technologies*, vol. 13, p. 6, 2021.

[31] R. Mailloux, *Phased Array Antenna Handbook*, Artech, New Jersey, NJ, USA, Second edition, 2005.

[32] Y. Tominaga, Y. Okamoto, S. Wakao, and S. Sato, "Binary-based topology optimization of magnetostatic shielding by a hybrid evolutionary algorithm combining genetic algorithm and extended compact genetic algorithm," *IEEE Transactions on Magnetics*, vol. 49, no. 5, pp. 2093–2096, 2013.

[33] K. Choi, D.-H. Jang, S.-I. Kang, J.-H. Lee, T.-K. Chung, and H.-S. Kim, "Hybrid algorithm combing genetic algorithm with evolution strategy for antenna design," *IEEE Transactions on Magnetics*, vol. 52, no. 3, pp. 1–4, 2016.

[34] H. Wei and X.-S. Tang, "A genetic-algorithm-based explicit description of object contour and its ability to facilitate recognition," *IEEE Transactions on Cybernetics*, vol. 45, no. 11, pp. 2558–2571, 2015.